New
Contaminants

Open Access

https://doi.org/10.48130/newcontam-0025-0001

Original Research

Polyethylene terephthalate microfiber release from textiles in coastal seawater ecosystems under sunlight-driven photochemical transformation

Rouzheng Chen[1], Xiaoli Zhao[1*], Xiaowei Wu[2*], Xia Wang[1], Junyu Wang[1] and Weigang Liang[1]

Received: 29 May 2025

Revised: 7 July 2025

Accepted: 8 July 2025

Published online: 5 September 2025

Abstract

Microfibers are ubiquitous in marine environments and are widely believed to be derived from synthetic textiles. While the forces driving microfiber formation in aquatic environments have yet to be clarified. In this study, we investigated the formation of polyethylene terephthalate (PET) microfibers released from textiles when subjected to long-term photoaging in coastal seawater environments. Results revealed that after 12 d of laboratory–accelerated UV irradiation, microfiber fragments were observed to be released from colored textiles. Specifically, 47,400, 37,020, 23,250, and 14,400 microfiber fragments were released from 0.1 g of purple, green, yellow, and blue textiles, respectively. This demonstrates that long-term photoaging can effectively convert PET textiles to microfiber. Furthermore, purple PET microfiber was demonstrated to have a higher photoaging rate compared to green, blue, and yellow ones, which is attributed to the dispersed dyes in purple textiles (0.0287) having higher light absorption than those in yellow (0.0237), blue (0.0252), and green (0.0287). Additionally, purple PET microfiber (6.20×10^{-15} M) generated more hydroxyl radicals than green, blue, and yellow microfibers (5.50×10^{-15}, 4.84×10^{-15}, and 4.17×10^{-15} M), which further accelerated the PET microfiber photoaging. The presented data offers new insights unraveling the formation and associated ecological risks of microfibers in coastal seawater environments.

Keywords: Microfiber, Photochemical transformation, Polyethylene terephthalate, Reactive oxygen species, Seawater

Highlights

- Long–term sunlight irradiation is susceptible to convert PET synthetic textiles to microfiber.
- 0.1 g of purple, green, yellow, and blue textiles could produce 47,400, 37,020, 23,250, and 14,400 microfibers during 12 d UV aging in seawater.
- Purple PET microfibers generated more of 6.20×10^{-15} M •OH than 5.50×10^{-15} M for green, 4.84×10^{-15} M for blue, and 4.17×10^{-15} M for yellow.
- Darker–colored PET microfibers (e.g., purple) exhibited 1.5–2.0 times faster photoaging rates compared to lighter colors (e.g., blue).

* Correspondence: Xiaoli Zhao (zhaoxiaoli_zxl@126.com); Xiaowei Wu (003836@nuist.edu.cn)
Full list of author information is available at the end of the article.

Graphical abstract

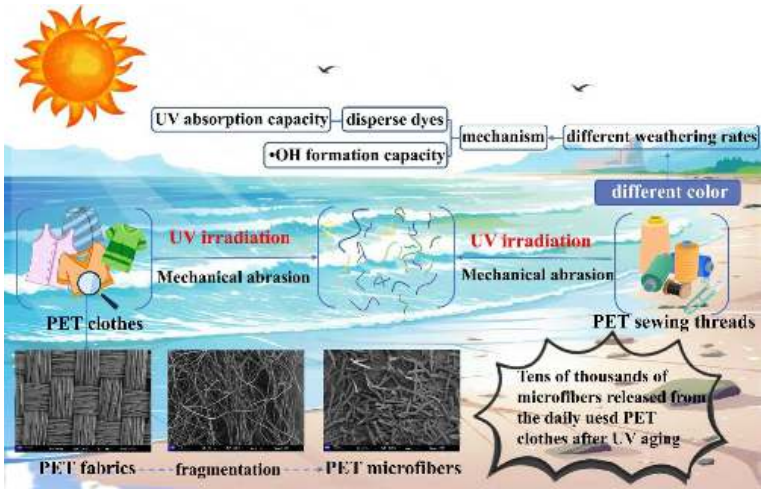

Introduction

Microplastics (MPs, plastic particles < 5 mm in size) have garnered significant concern in marine environments, and are acquiring increasing concern[1], due to their persistent organic pollutants (POPs)–like characteristics, including environmental persistence, bio-accumulation potential, long–range transportability, and ecotoxicological risks[2]. Coastal ecosystems act as major sinks for land–based plastic waste, with 20–53 million metric tons entering marine waters annually via runoff and atmospheric deposition[3,4]. According to current knowledge, many efforts have demonstrated the extensive occurrence of microplastic pollution in current marine seawater through *in situ* monitoring, with the concentration varying from 0.02 to 8,500 n/m^3 (Supplementary Table S1). In comparison with spheres, fragments, and firm microfibers, synthetic filaments with a length: diameter ratio > 3[5], are the primary contributor to marine microplastics, contributing for 21.9 to ~100 of total microplastic accumulation (Supplementary Table S1)[6]. In addition, microfibers are of higher toxicity and ecological risks to marine organisms than those of granular or film MPs due to their slender shape and readily ingested by marine organisms such as zooplankton, clams, shrimp, fish, and invertebrates[7–9]. Hence, in-depth investigations into the source and ecology of marine microfibers are urgently needed[10].

During long-term retention in marine environments, microfibers are readily able to endure long-term biotic and abiotic weathering processes, including hydrolysis, mechanical abrasion, photoaging, biodegradation, and thermal oxidation, with ultraviolet (UV) irradiation–induced photoaging regarded as an essential contributor to plastic fragmentation and microplastic formation. For instance, Bai et al. found that 1 mm^2 of polyethylene terephthalate (PET) geotextile could generate up to 2.52 × 10^6 microfibers after 35 d of UV aging using a mercury lamp (256 W/m^2)[11]. Pinlova & Nowack utilized xenon arc exposure with irradiance maintained at 60 W/m^2 (total UV) to weather different textiles, and found that 1 g of textile led to the release of 160–450 × 10^3 microfibers[12]. This is due to the continuous UV exposure facilitating the plastic polymer chain succession, leading to the embrittlement of plastic debris, and tends to break into smaller–sized microfibers[13].

The mechanism associated with the UV irradiation triggered the plastic polymer chain cleavage is assigned to the direct photo-oxidation of plastics when polymer absorbed more of UV energy than that of bond dissociation energy, such as C–C bond (375 kJ/mol) and C–H bond (420 kJ/mol), and subsequently lead to the polymer chain cleavage[14,15]. Additionally, various reactive oxygen species (ROS) (i.e., hydroxyl radical (•OH), superoxide anion ($\bullet O_2^-$), singlet oxygen ($^1O_2$), and hydrogen peroxide (H_2O_2)) generated by MPs under UV irradiation catalyze radical chain reactions, further promoting the cleavage of polymers (referred to as free radical-sensitized photooxidation)[16]. Moreover, continuous photochemical transformation of microfibers in the seawater environment can induce the release of micro- and nano-scale aged plastic debris[1,17] and toxic chemicals (additives and oligomers)[18–20], which simultaneously pose a health threat to marine life and biodiversity through ingestion[21]. Therefore, the environmental behavior of photodegraded microfibers in the marine environment should be seriously considered.

Among varied microfiber residues in marine environments, synthetic textiles, particularly colored PET fabrics, are a growing concern which are widely used in textiles (e.g., clothing, curtains, and carpets) due to their durability and low cost[22], and readily enters into the environment through domestic emission, a single household laundry cycle releases ~730,000 microfibers[23]. Emission of PET fiber can subsequently enter into marine ecosystems through river surface runoff and act as an essential contributors to total fiber accumulation in marine environments. Therefore, investigating the formation and fate of marine PET microfiber, a representative of microfiber and even microplastics, is crucial for assessing their ecological risk in marine ecosystems. Microfiber residues in current marine environments are of different colors (i.e., black, blue, transparent, and red). It has been previously reported that microfiber in the Northwestern South China Sea iss composed of blue (59%), and black (28%), with microfiber in Argentina's sea composed of black (38%), blue (22%), and red (16%), respectively[24]. Hence, the synergistic effect of colored pigments or dye residue in altering PET microfiber photodegradation kinetics in seawater can not be ignored and has yet to be resolved.

In this study, we focused on the sunlight–driven photochemical transformation of textiles to microfibers in coastal seawater environments and then compared the differential photochemical fates of colored microfibers in aquatic waters. Specific objectives of this work are to unravel: (i) how long-term UV exposure drives PET textile fragmentation and microfiber release in coastal seawater; (ii) why

colored microfibers exhibit differential photoaging kinetics, with a focus on dye-mediated reactive oxygen species (ROS) generation; (iii) whether darker-colored PET microfibers (e.g., purple) degrade faster due to enhanced UV absorption and ROS production compared to lighter colors (e.g., yellow). The obtained findings herein may help unravel the formation mechanism, fate, and potential ecological risk of colored microfibers in marine environments.

Materials and methods

Materials

All of the PET textiles (plain staple fabric, woven structure) were confirmed to have identical yarn density (120 threads/cm^2), and polymer composition via FTIR (Supplementary Fig. S1). No additional finishes (e.g., flame retardants) were applied, ensuring color (disperse dyes) was the sole variable. PET textiles and sewing threads (type: 402) were purchased from Suzhou Yunheng Textile Co., Ltd., China. The textiles were dyed with industry–standard disperse dyes: CI Disperse Yellow 54 (C.I. 47020, anthraquinone–based), Disperse Brilliant Green 5GL (C.I. 61570, azo-based), CI Disperse Blue 60 (C.I. 61105, anthraquinone-based), and CI Disperse Violet 63 (C.I. 11120, nitro-based) (Supplementary Table S2). These dyes were selected for their widespread use in PET textiles and distinct light absorption properties (Supplementary Fig. S1). The coastal seawater used in this study was sampled in Weihai (Shandong Province, China) (122°1′10″ E, 37°31′7″ N) on October 24, 2022 (Supplementary Fig. S2). The basic water qualities were pH: 6.45; salinity: 22.4 g/L; conductivity: 12.9 μS/cm; and total organic carbon: 3.51 mg/L. Nitrobenzene (NB, $C_6H_5NO_2$, 123.11 g/mol), and isopropanol (IPA, C_3H_8O, 60.10 g/mol) were purchased from Makline Co., Ltd. (Shanghai, China).

UV irradiation experiments

Accelerated UV irradiation experiments were employed to mimic the weathering process of fibers. Pristine PET (100 mg) and coastal seawater (15 mL) were mixed in transparent quartz tubes, which were placed in a photochemical reaction apparatus (CEL–LAB500; Beijing Zhongjiao Jinyuan Technology Co., Ltd., China) and UV irradiated for 2, 4, 6, 8, 10, and 12 d, respectively. The 500 W mercury lamp (260–600 nm emission spectrum) provided a UV intensity of 100 W/m^2 at 365 nm, covering 85% of natural solar UV radiation (UVA: 315–400 nm; UVB: 280–315 nm) at mid–latitude coastal regions[25]. Based on cumulative UV dose equivalence, 12 d of laboratory aging simulated 365 d of real-world natural sunlight in marine environments (calculated as 30 MJ/m^2 total UV energy)[13]. A magnetic stirrer with a consistent rotation speed of 500 rpm was selected to generate turbulent flow simulating shear forces equivalent to wave action in shallow coastal zones. The velocity of the stirrer was equivalent to the water velocity of 2.12 m/s ($V = 0.25 \times n + 0.010$, n is the mechanical stirrer rotating speed), and within the range of water velocity in the sampling area (0.50–3.00 m/s in Weihai, Shandong Province, China) (www.weihai.gov.cn)[26].

Additionally, the temperature of the seawater during the experiment was controlled at 20 °C (temperature of surface water) by circulating condensate. Note that the microfibers released from PET textiles were collected using a 3 μm stainless steel filter membrane, with the pore sized of filter relatively lower than that of marine microfibers in current marine waters (such as the Atlantic Ocean, Southern Ocean, and Indian Ocean), with the median microfiber length and diameter were 1.07 mm (range, 0.09–27.06 mm), and 16.7 μm (range 5 to 239 μm), indicating that the 3 μm stainless steel filter is available for capturing relevant microfibers released by textiles. The quenching experiment procedure was conducted using 400 mM isopropanol (IPA) as the •OH scavenger, which readily achieved > 95% radical quenching efficiency at this concentration according to our prior exploration[27].

Instrumental analysis

The masses of pristine and aged PET fibers were determined using a precision balance (FA604B; Shanghai Precision Instruments Co., Ltd, China). The PET fiber length in seawater was measured using a microscope imaging system (Leica Microsystems, Wetzlar, Germany). SEM imaging (Hitachi S–4800) was performed at 5 kV accelerating voltage, 10 mm working distance, and 5,000 × magnification. Samples were gold–sputtered (10 nm thickness) to enhance conductivity. Microscope imaging (Leica) utilized a 40 × objective lens (NA 0.75) with 0.5 μm resolution. Changes of PET color were quantified using a spectrocolorimeter (DS–200; Hangzhou Color Spectrum Technology Co., Ltd., China). The obtained spectrum was further converted to chromaticity values (L*, a*, and b*), and differences between the colors of the two samples were calculated based on their chromaticity values using Eq. (1)[28].

$$\Delta E = \sqrt{(L_1^* - L_2^*)^2 + (a_1^* - a_2^*)^2 + (b_1^* - b_2^*)^2} \quad (1)$$

where, ΔE is the color difference between objects 1 and 2; L* refers to the plastic brightness (L* 0 and 100 refers to black and white color); a* refers to the chroma (positive a* value denotes redness while a negative a* value denotes greenness); b* refers to the saturation (positive b* value denotes yellowness while a negative b* value denotes blueness)[29].

Fourier–transform infrared (FTIR) spectroscopy was carried out using an attenuated total reflection probe (Cary 630 FTIR, Agilent Technology, Santa Clara, USA). Spectra were recorded from 4,000 to 600 cm^{-1} with a spectral resolution of 4 cm^{-1}, taking the average of 32 scans. Plastic aging extent associated CI (carbonyl index) values, which reflects the formation of carbonyl oxidation products on the sample surface (e.g., carboxylic acids, ketones, aldehydes, lactones, and esters), for pristine and aged PET were calculated as the ratio between the absorbance of the carbonyl group at 1,712 cm^{-1} (C=O stretching) and that of an unalterable band (1,407 cm^{-1}).

Quantification of PET photoaging–associated free radicals

NB was used to quantify •OH generation by PET threads and dyes under UV irradiation[26]. In the capture system for •OH, 100 mg of PET threads and 20 mg dye were added to 30 mL of seawater containing 2 mM NB. During the light experiment, 0.5 mL aliquots were removed at 0, 1, 2, 3, 4, and 5 h, and matrix effects from seawater were minimized by pre–filtering samples through 0.45 μm glass fiber membranes. The accumulated •OH concentration within the reaction system was quantified via HPLC (Agilent 1200). According to the instrumental manufacturer, the detection limit of HPLC is 0.1 μM and the linear range is 0.5–50 μM ($R^2 > 0.99$). In addition, the triplicate injections ensured < 5% relative standard deviation. HPLC coupled with a C18 reversed-phase column (5 μm × 250 mm × 4 mm) and UV–Vis detector. The mobile phase contained acetonitrile and water (60:40 v/v) at a flow rate of 0.5 mL/min. The injection volume, detection wavelength, and temperature were set at 10 μL, 263 nm, and 30 °C, respectively[30]. The steady-state •OH concentration ($[•OH]_{SS}$) was calculated by linearly fitting the loss of NB in the presence of different colored PET threads at different UV-induced aging times using the following equation[31]:

$$[\bullet OH]_{SS} = k'_{NB}/k_{NB-\bullet OH} \quad (2)$$

where, k'_{NB} is the first–order kinetic constant of NB consumption, and $k_{NB-\bullet OH}$ is the second-order kinetic constant of the reaction of NB with •OH (3.9×10^9 M/s).

Statistical analysis

Note that experiments related to the microfiber photoaging, characterization (i.e., fiber length, mass CI value, and chromaticity), and ROS (•OH) quantification were repeated in triplicate (n = 3), and the obtained results were supplied by average values coupled with standard deviation. Statistical analysis for the changes of microfiber size, carbonyl index, and NB concentration (used for •OH quantification) vs UV aging time was fitted using Origin 2018 software.

Results and discussion

Photoaging of PET synthetic textiles induced the release of microfibers

The original PET textile surface comprised a mesh structure formed by interweaving two sets of perpendicular threads in the warp and weft. SEM revealed progressive structural degradation of PET textiles under UV exposure, with microfiber shedding initiating from warp–weft intersections (Fig. 1a). Similarly, extensive cracks create abundant, tiny, fragmented particles on the surface of plastic materials (Fig. 1b)[32]. After 12 d, the original mesh structure fragmented into detached fibers and caused higher turbidity to the surrounding water during the photoaging process, with no difference observed in dark controls (Supplementary Fig. S3).

In addition, 0.1 g of different colored PET textile released $1.44–4.74 \times 10^4$ microfibers of UV irradiation in coastal seawater. The observed microfiber release aligns with studies on polyester laundry shedding (Pinlova et al.[22]: $160–450 \times 10^3$ items/g) but is significantly lower than geotextile fragmentation rates (Bai et al.[11]: ~1.83×10^9 items/g, calculated based on PET density). This discrepancy may stem from structural differences: loose textile fabrics release fewer fibers under UV aging compared to mechanically stressed geotextiles. This discrepancy arises because the loose fiber network of textiles dissipates stress and allows deeper UV penetration, leading to gradual bulk oxidation rather than surface–layer spallation observed in dense geotextiles. Additionally, the number of microfibers shed from the purple textile into seawater (47,400 particles) was significantly higher than that shed by the green (37,020 particles), yellow (23,250 particles), and blue (14,400 particles) textiles. From this point of view, structural damage caused by long-term sunlight irradiation of PET textile in marine surface water is responsible for releasing abundant smaller–sized secondary microfibers and further polluting the seawater[32].

Supplementary Fig. S4a and S4b showed that, in comparison with pristine PET textile (3,000–5,000 μm), fragmented microfibers ranged from 200–2,000 μm (Fig. 2a), with purple PET producing the smallest median size (1,575 ± 26 μm), followed by yellow (1,553 ± 48 μm), blue (1,835 ± 32 μm), and green (2,391 ± 194 μm) (Supplementary Table S3). Meanwhile, nano-sized fibers were sized in 0.42 μm (yellow textile), 0.31 μm (green textile), 0.89 μm (blue textile), and 0.48 μm (purple textile), respectively (Fig. 2b, e). These results stressed that plastic fragments derived from PET can further break into smaller-sized microfibers and further pollute coastal seawater.

Key role of color in the differential PET microfiber photoaging rates

long-term photoaging of PET textiles in coastal seawater is also prone to fading the color of textiles gradually, and the threads on the textile edge protrude and entangle with one another, with fibers constantly falling off, leaving the textile edge rough, rounded, and light gray or white (Supplementary Fig. S3). As shown in Fig. 3, L* values were almost unchanged for the textiles after 12 d of UV exposure, except for the purple textile. The decreased b* value of the yellow textile and increased b* value of the blue textile indicated loss of original color. This was consistent with the increased a* value of the green textile. UV–induced aging had a significant effect on the purple textile, with the largest variations in L*, a*, and b* values among the colored textiles. Compared to the initial color, the purple textile exhibited a higher color difference (23.37 ± 1.49), followed by the blue textile (16.69 ± 0.60), with an exiguous difference between the green (12.61 ± 0.51), and yellow (11.21 ± 0.53) textiles was found (Table 1). In addition, UV light had a considerable influence on the color fastness of the textiles[33]. Color fastness, which refers to the degree of color fading of dyed textiles under the action of external factors (e.g., friction, washing, UV exposure), can determine the performance level of particular dyes or colorants for textile applications[29].

This property is critically influenced by dye-substrate interactions and environmental stressors, as demonstrated in standardized testing protocols (ISO 105-B02:2014. www.iso.org). It is usually divided into grades 1–5, with a higher grade indicating stronger resistance to external forces and ability to maintain the original color[29]. After UV exposure, all textiles exhibited poorer resistance against UV light compared to the original textiles, with the purple textile demonstrating the greatest reduction in color fastness (from grade 4 to grade 2). This is attributed to the presence of less dye in the textile due to dye oxidation after long-term UV exposure.

In Supplementary Fig. S5a, when the PET microfiber underwent photoaging in coastal seawater, the yarn structure was destroyed and abundant individual fiber filaments were formed, and then broke into sections of microfibers with smaller lengths, and the fiber ends exhibited splitting, flattening, and roughness. No surface features related to weathering were found on pristine fibers or those under dark conditions (Supplementary Fig. S5b), suggesting that different colored PET microfibers are subject to endure photoaging and fragmentation process and consistent with that of PET textiles (Fig. 1). Diverse photoaging rate of different colored PET microfiber were further investigated by comparing the changes of polymer mass, size distribution, chromatic aberration (ΔE), oxygen content, and crystallinity. No differences were discovered for the changes of PET microfiber structures (i.e., mass, size, and CI) under darkness controls (Fig. 4).

Figures 4a, b showed that purple PET microfiber exhibited higher mass loss (38.2%) than that of green (35.0%), yellow (31.4%), and blue (22.4%). In contrast, polymer size associated changes in the fragmentation ratio (ln (S_t/S_0, S_t: microfiber size at aging time t, S_0: initial microfiber size) of PET threads were calculated (Fig. 4c), with the linear correlation coefficients fitted with the absolute ratio were 2.70×10^{-1}, 2.71×10^{-1}, 2.67×10^{-1}, and 2.52×10^{-1} for purple, green, yellow, and blue PET microfiber, respectively. In addition, the ΔE values of different colored PET microfibers were compared to illustrated diverse photoaging ratio of colored PET microfiber based on the continuous changes of L*, a*, and b* values during 12 d UV irradiation in seawater (Supplementary Fig. S6), with the specific calculation strategies supplied previously. The obtained results showed that purple PET microfiber showed higher color difference

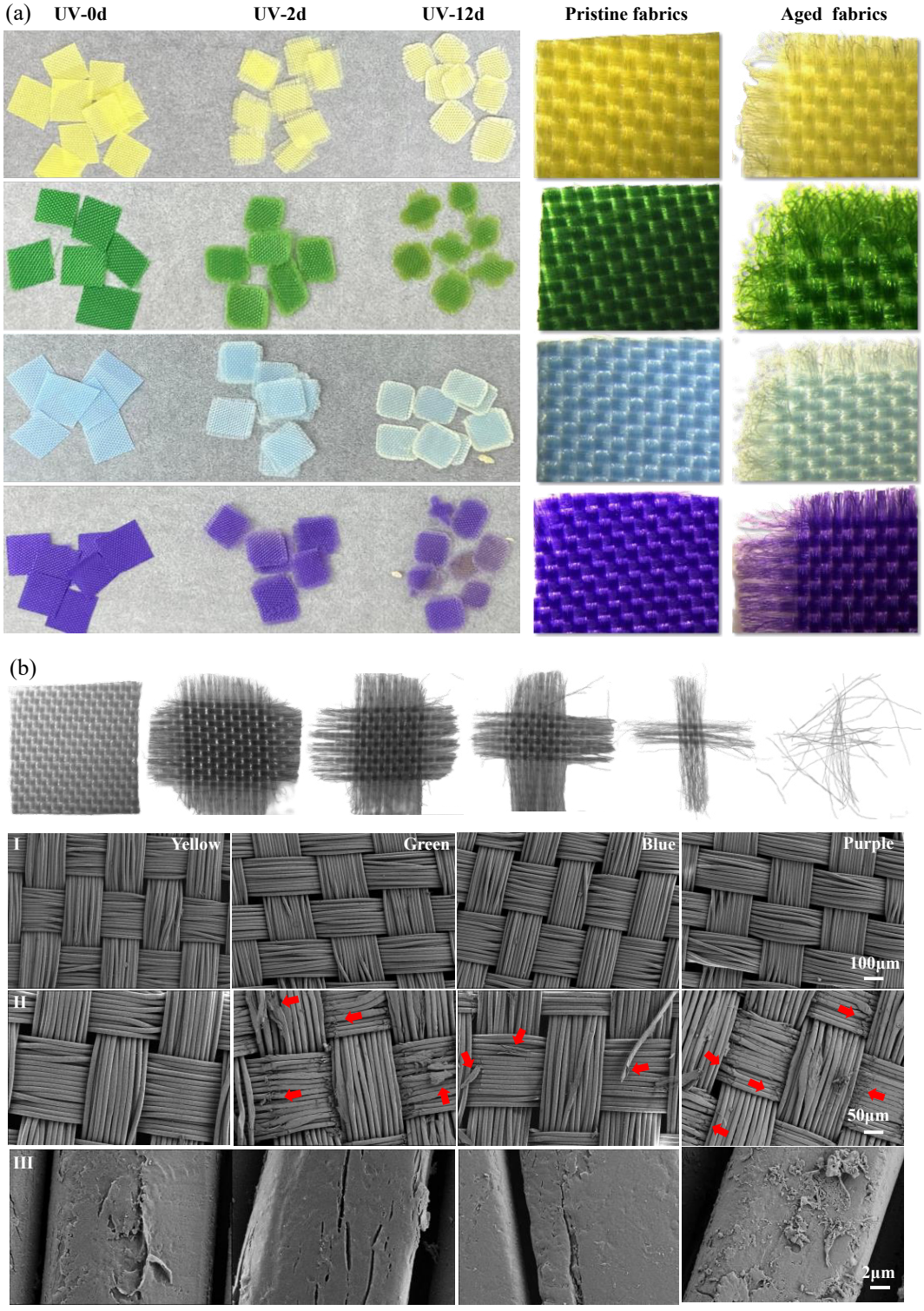

Fig. 1 (**a**) Morphology and appearance changes of the four color of PET texitles after UV exposure under a microscope. (**b**) Different shapes of textiles during the weathering process.

(ΔE: 36.13 ± 1.79) than those of green (ΔE: 33.7 ± 0.03), yellow (ΔE: 30.26 ± 0.54), and blue (ΔE: 30.8 ± 1.28) (Fig. 4d), revealing that purple PET microfiber equipped higher photoaging ratio in coastal seawater than those of green, yellow, and blue ones during long-term photoaging in coastal seawater matrices.

The effect of colored pigments on the PET microfiber weathering was also verified through the CI and crystallinity. PET microfiber aging extent associated CI value was calculated via carbonyl group at 1,712 cm^{-1} (C=O stretching) and that of an unalterable band (1,407 cm^{-1}) based on the ATR–FTIR results (Fig. 5a). During 12 d of UV irradiation, the CI values of the different colored PET microfibers increased continuously, evidencing the continuous formation of carbonyl oxidation products on the sample surface (e.g., carboxylic acids, ketones, aldehydes, lactones, and esters), with purple

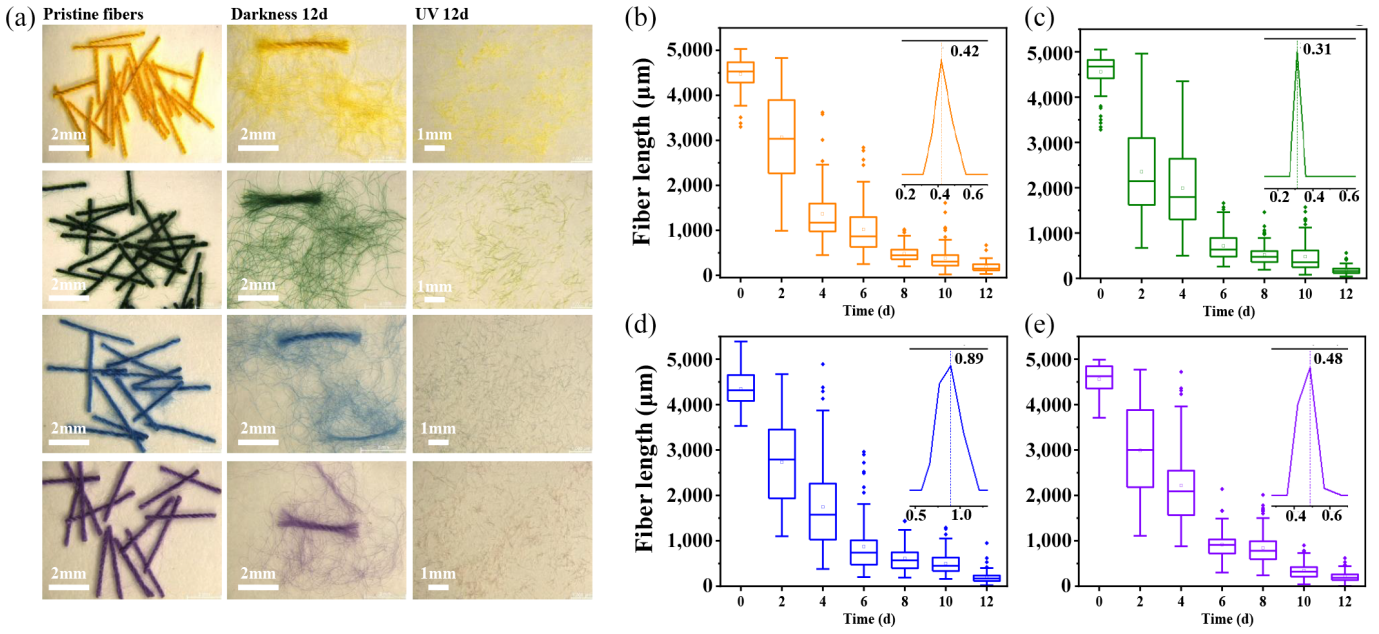

Fig. 2 (**a**) Microscope image associated to the photoaging induced fragmentation of different colored PET microfiber in coastal seawater. Size distribution of different colored PET microfibers (**b**) yellow, (**c**) green, (**d**) blue, (**e**) purple, during UV aging in coastal seawater.

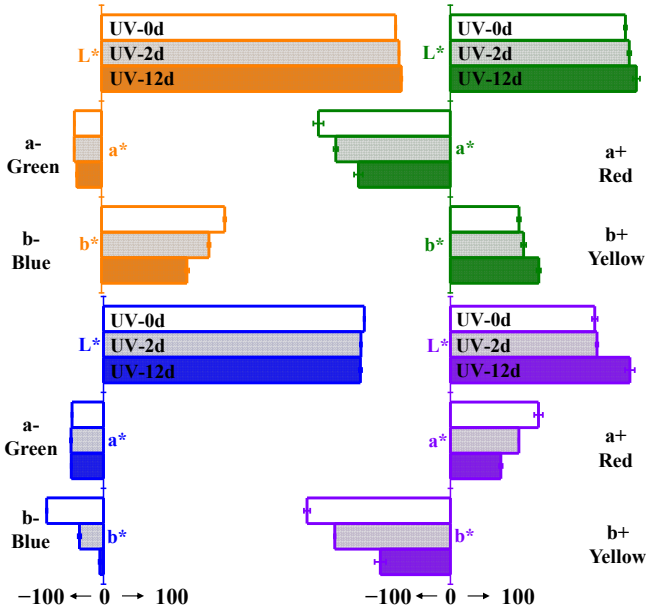

Fig. 3 Chromaticity value changes of textiles with different colors after UV exposure.

Table 1 Chromogenic performance of different color textiles after UV exposure

Textile color	Pirstine	Dark 12 d	UV exposed				Grade (staining fastness)	
			2 d	ΔE	12 d	ΔE	2 d	12 d
Yellow				5.56 ± 0.19		11.21 ± 0.53	4–5	4
Green				6.73 ± 0.34		14.61 ± 0.51	4	2–3
Blue				9.62 ± 0.26		16.69 ± 0.60	4	3
Purple				8.39 ± 0.23		23.37 ± 1.49	4	2

microfiber (2.69 ± 0.05) displayed was higher CI value than that of green (2.63 ± 0.05), yellow (2.59 ± 0.04), and blue (2.58 ± 0.02) (Fig. 5b).

In addition, the changes of CI value for different colored PET microfiber were also fitted through pseudo-first-order kinetics, with the increase rate for purple PET microfiber (1.80×10^{-2} d^{-1}) was higher than those of green: 1.50×10^{-2} d^{-1}; blue: 1.30×10^{-2}; and yellow: 1.10×10^{-2} d^{-1} (Fig. 5c). In terms of the PET microfiber crystallinity, reflecting the polymer molecular chain arrangement, was calculated by A_{1340} (C–H out-of-plane oscillating vibration) to A_{1407} (reference peak) absorption peak intensity ratio based on the ATR–FTIR results (Supplementary Fig. S7). In comparison with dark controls (Fig. 5d), the A_{1340}/A_{1407} value decreased continuously (Fig. 5e), with the purple, green, yellow, and blue PET microfiber decreased by 11.78%, 11.78%, 7.66%, and 3.27%, respectively, which reflected the long-term UV aging induced higher amorphous region on the PET microfiber surface (Fig. 5e). This may attribute to the fact that photoaging–induced oxidation of the end or side chains of polymer chains and the formation of functional groups, such as hydroxyl and carbonyl groups, causing weaker interactions between molecules, making the molecular structure more flexible, and resulting in decreased crystallinity of polymer molecular chains[34].

Subsequently, we fitted the changes of different colored PET crystallinity during photoaging in coastal seawater environments through first–order kinetics (correlation coefficients > 0.99), which assistant with the changes of polymer mass, size distribution, chromatic aberration (ΔE), and CI, the purple PET microfiber (1.50×10^{-2}) displayed higher decrease rate for crystallinity than that of green (0.90×10^{-2} d^{-1}), yellow (0.20×10^{-2} d^{-1}), and blue (0.90×10^{-2} d^{-1}) PET microfiber (Fig. 5f). Those highlighted varied photoaging rates of different colored MPs during long-term retention in coastal seawater, with purple PET microfiber equipping a higher

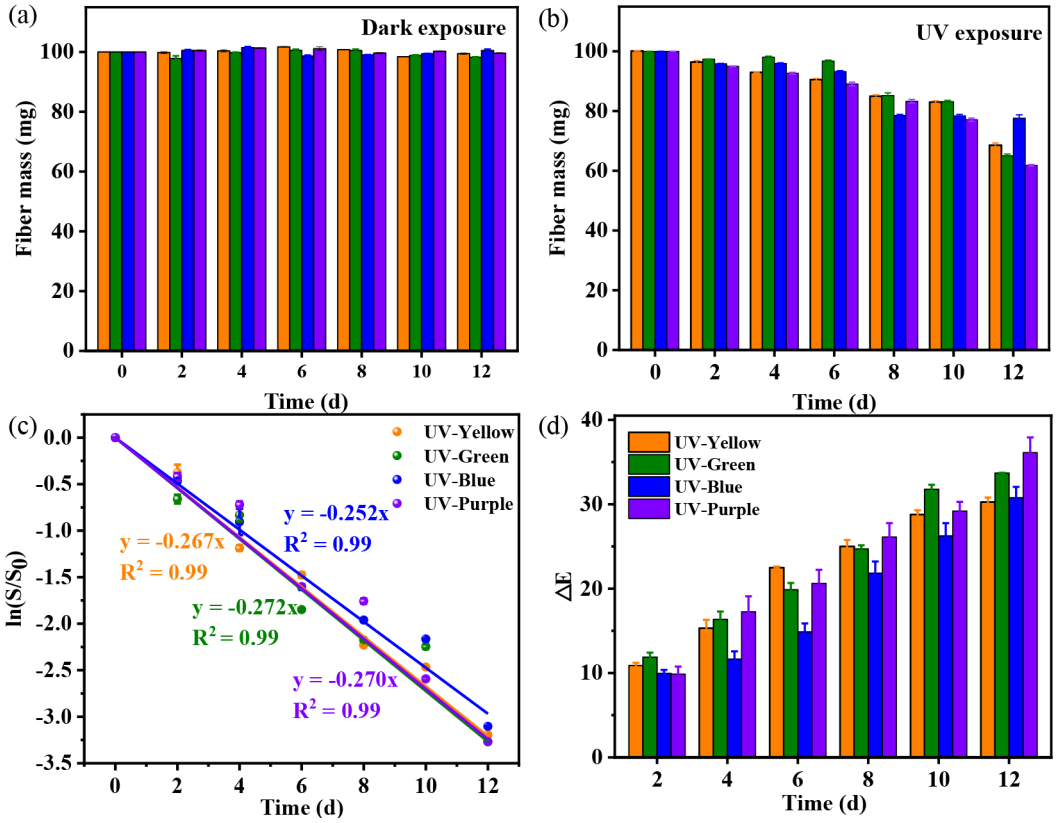

Fig. 4 Mass changes of different PET sewing threads under (**a**) dark, and (**b**) UV light conditions. (**c**) Changes of fragmentation ratio of different PET microfiber during photoaging in coastal seawater. (**d**) Chromatic aberration (ΔE) of different colored PET microfiber during UV light irradiation in seawater matrices.

photoaging rate than other colors of blue, green, and yellow species. Subsequently, the photoaging mechanisms of different colored PET microfibers in coastal seawater were further investigated.

Mechanism illustrating color–dependent PET fibers photoaging in coastal seawater

The photoaging mechanism of MPs in aquatic environments mainly includes direct photooxidation, which refers to direct internal breakage of polymer chains when the energy of UV light absorbed by the plastic is greater than the bonding energy of the compound and free radical-based photooxidation, which refers to the chain reaction of free radicals generated by MPs leading to decomposition of the polymer[35]. In terms of direct photooxidation, we explored the effect of colored disperse dyes (yellow: CI Disperse Yellow 54; green: Disperse Brilliant Green 5GL; blue: CI Disperse Blue 60; and purple: CI Disperse Violet 63), which commonly adhered onto PET fiber via H–bonds and van der Waals forces[5], on the PET microfiber UV absorption capacity (190–400 nm) during the photoaging process (Supplementary Table S3). In Supplementary Fig. S8, the average absorbance of disperse yellow, green, blue, and violet dyes at 190–400 nm gradually increased with increased dye concentration. Additionally, plots of absorbance vs dye concentration for the different dyes displayed linear relationships, with all adjusted correlation coefficients (R^2) > 0.99. The absorption capacities of green (equilibrium constant a: 2.80 × 10^{-2}) and purple (a: 2.70 × 10^{-2}) dyes were greater than those of yellow (a: 2.40 × 10^{-2}) and blue (a: 2.50 × 10^{-2}) dyes, indicating that green and purple dyes can absorb more UV light during the aging process and thus promote the aging of PET plastic.

Free radical–sensitized (•OH, $O_2^{\bullet-}$, and $^1O_2$) oxidation of MPs have been demonstrated to be a dominant process controlling the photoaging mechanism of plastics in coastal seawater, with •OH is of higher oxidation capacity (redox potential is 2.7 V) when degrading organic chemicals in comparison with those of $O_2^{\bullet-}$, $^1O_2$, etc[36]. Under UV light exposure, MP polymer (RH) readily absorbs UV light photons and forms hydroperoxides (ROOH), which are further cleaved into alkoxy radicals (RO•) and •OH[37]. The produced •OH then will attack the polymer chain (RH) (RH + •OH → R• + H_2O) through hydrogen abstraction, addition, or hydrolysis reactions, leading to the plastic polymer fragmentation and ultimately degradation of the plastic material[38]. Hence, •OH catalyzed photoaging of PET microfiber in coastal seawater was investigated to unravel the color-dependent diverse PET photoaging mechanism in coastal seawater. Sampled as purple PET microfiber, in comparison with pristine PET microfiber, after 72 h of UV irradiation, the CI value of PET increased by 2.59 ± 0.02 in seawater, which was fairly higher than that of IPA + seawater (2.28 ± 0.09), evidencing that the •OH played an important role in the photoaging of PET microfiber in coastal seawater (Supplementary Fig. S9).

To further clarify the color–dependent PET photoaging mechanism in coastal seawater, we compared the •OH formation capacity of different colored PET threads. The •OH triggered plastic polymer chain succession under UV irradiation is associated with the •OH, which could attack the C–H bond in the polymer to form alkyl radicals (R•), and H_2O (•OH + RH → R• + H_2O). Qualitative analysis for the •OH formation by PET microfiber (sampled as purple and green) in seawater was explored through electron spin resonance (EPR) using 5,5-dimethyl-1-pyrroline-N-oxide (DMPO) spin–trapping. As

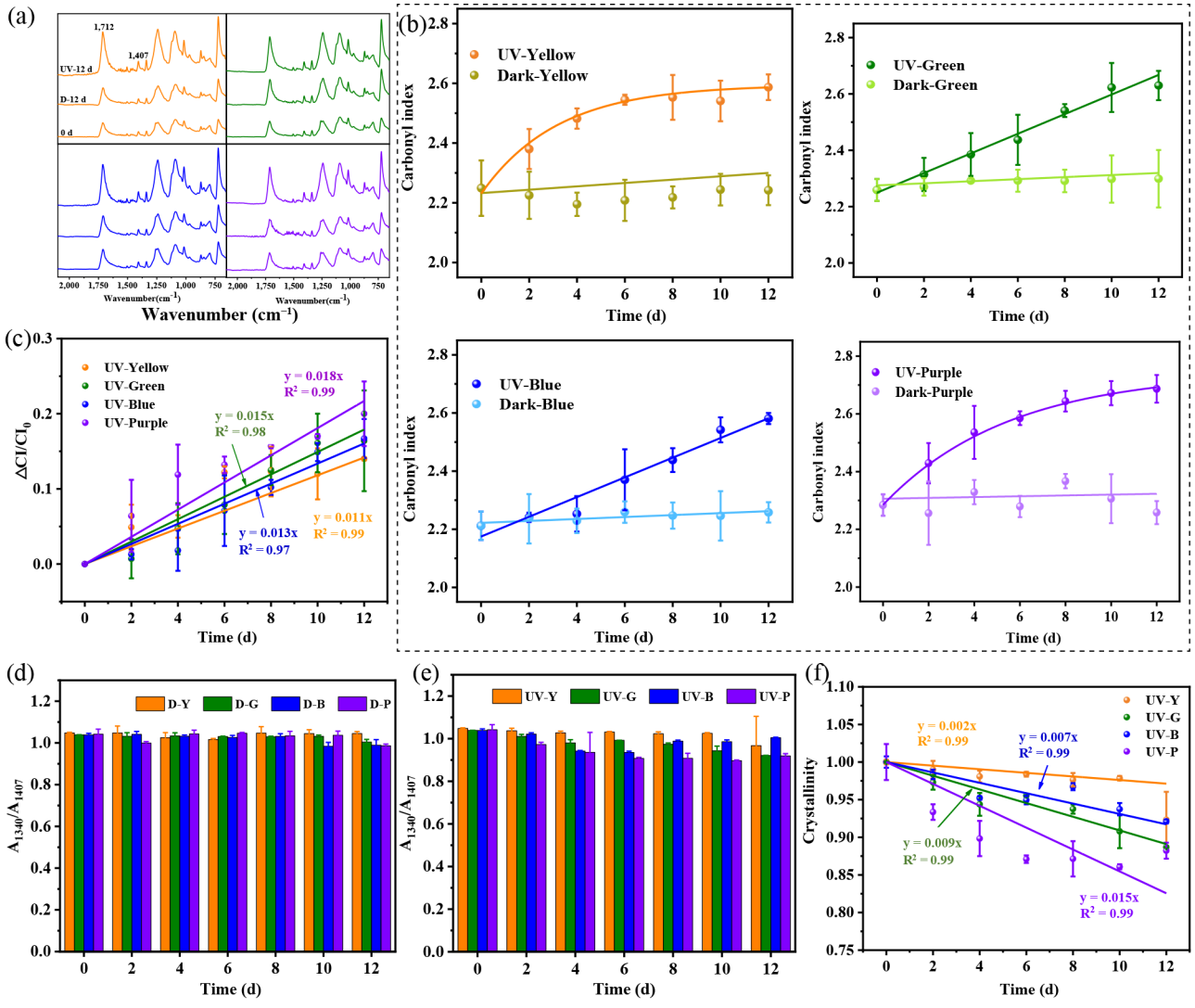

Fig. 5 (**a**) FTIR spectra, and (**b**) carbonyl index of different colored PET microfibers within 12 d treatment under UV light and darkness conditions. Crystallinity changes of different colored PET microfibers within 12 d treatment under (**d**) darkness conditions, and (**e**) UV light. Fitting results of (**c**) increased CI, and (**f**) crystallinity with aging time for different colored PET.

shown in Fig. 6a and b, the typical DMPO–OH signal (with a peak intensity ratio of 1:2:2:1) of PET threads was observed after 20 min of UV exposure, and no peaks were observed for threads under dark conditions, which suggested that photoaging of different colored PET in coastal seawater induces •OH formation[39]. Subsequently, the •OH formation capacity of different colored PET threads under UV irradiation was compared using NB solution (Fig. 6c). No significant changes were observed between pristine PET threads and those under dark conditions, whereas the NB concentration gradually decreased for different colored PET threads under UV irradiation. The consumption ratio of NB in the UV reaction system was higher for purple PET thread (k'_{NB}: 8.71 × 10^{-2} h^{-1}) than for other colors (green: 7.72 × 10^{-2} h^{-1}, blue: 6.79 × 10^{-2} h^{-1}, and yellow: 5.85 × 10^{-2} h^{-1}). Correspondingly, the •OH concentration produced by purple thread under light exposure was higher (6.20 × 10^{-15} M) than that by other colors (green: 5.50 × 10^{-15} M, blue: 4.84 × 10^{-15} M, and yellow: 4.17 × 10^{-15} M).

The presence of additives, such as dyes, is considered a starting point for radical reactions caused by UV irradiation. Photosensitization by dye molecules takes place under visible light irradiation, which has been successfully applied to degrade dye pollutants[40]. Studies have revealed that •OH is the main reactive species for dye removal, and it non-selectively reacts with most organics until mineralization occurs, i.e., their transformation into CO_2, water, and inorganic ions[41,42]. Disperse dyes play a vital role in accelerating •OH generation by PET plastic. When it comes to the chemical structure-dominated formation of •OH by colored dyes. Existing efforts showed that, under sunlight irradiation, the C–H bond in the organic dye (RH) (yellow, green, blue, and purple) is prone to cleavage and forms alkyl radicals (R•) firstly[36]. Then the formed R• in water is readily able to react with oxygen or dissolved oxygen in the water, producing alkoxy radicals (RO•) and alkyl peroxy radicals (ROO•). Furtherly, ROO• could react with hydrogen in water to generate hydroperoxide (ROOH), which decomposes into alkoxy radical (RO•) and produces •OH[43].

Similarly, the EPR spectra results (Fig. 6e, f) showed that different disperse dyes produced •OH after 20 min of light exposure, and no difference was observed between pristine PET threads and those under dark conditions (Supplementary Fig. S10). The same method was employed to obtain the absolute first–order rate constants of consumed NB by different dyes at different times (k'_{NB}: purple 11.89

× 10^{-2} h^{-1}, green: 11.51 × 10^{-2} h^{-1}, blue: 10.66 × 10^{-2} h^{-1}, and yellow: 9.64 × 10^{-2} h^{-1}). Subsequently, the formation capacities of •OH by disperse yellow, green, blue, and purple dyes were calculated to be 6.87 × 10^{-15}, 7.59 × 10^{-15}, 8.20 × 10^{-15}, and 8.47 × 10^{-15} M, respectively.

These results indicated that purple and green dyes have higher capacities to produce •OH than blue and yellow dyes. Overall, the results indicated that prolonged photoaging of PET textiles are available to release abundant secondary microfiber to the surrounding seawater (Fig. 7). Corresponding for the purple microfiber displayed higher photoaging rate in coastal seawater, followed by green, and finally blue and yellow with little difference (Fig. 7). The proposed mechanism was mainly attributed to the stronger ability of purple dye to absorb ultraviolet rays. Meanwhile, purple fibers and dyes could produce more free radicals under UV irradiation, further promoting the weathering of purple PET fibers.

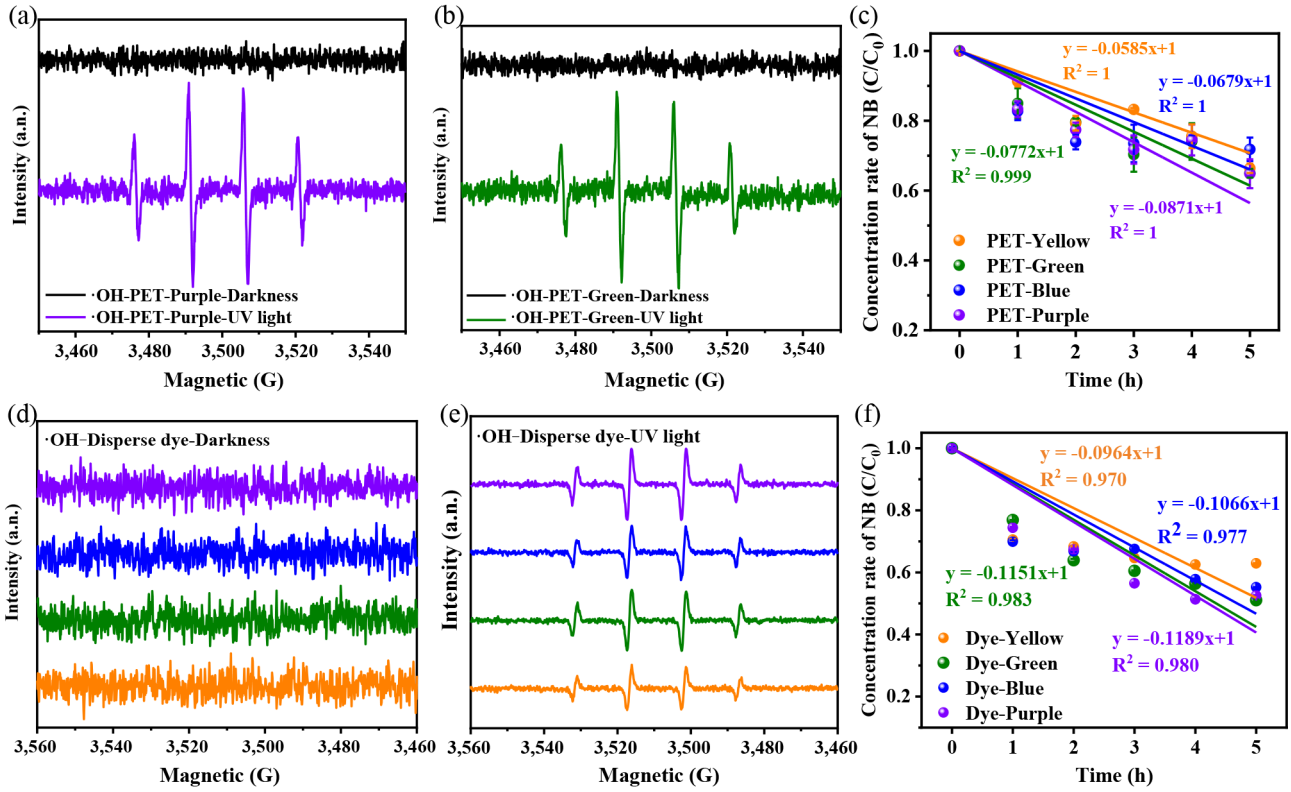

Fig. 6 EPR spectra of (**a**) purple, (**b**) green, and different disperse dyes under (**d**) darkness and (**e**) UV light conditions. Quantification analysis for the (**c**) •OH formation of different colored PET microfibers, and (**f**) different disperse dyes under UV irradiation.

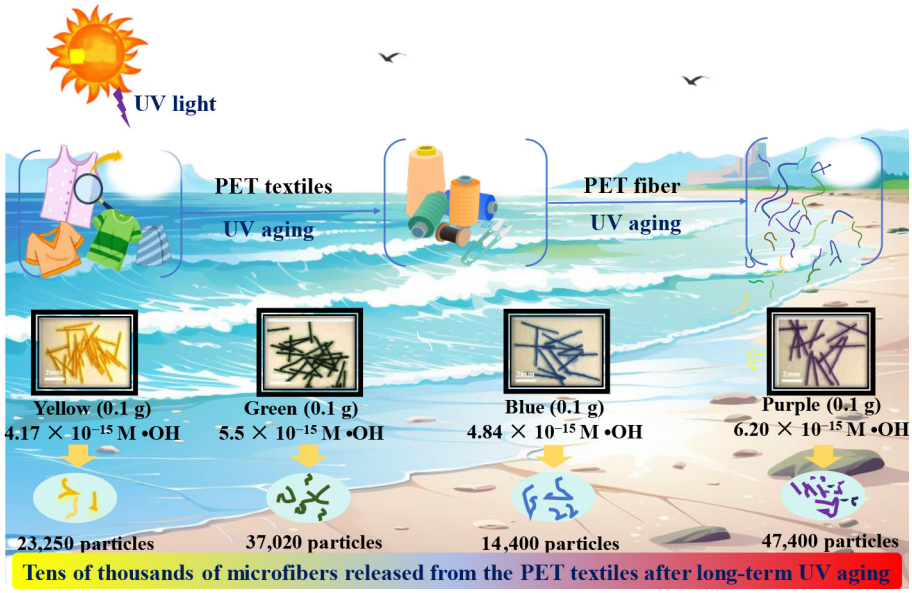

Fig. 7 Scheme for the prolonged photoaging of different colored PET textiles induced PET microfiber release into surrounding coastal seawater.

Conclusions

Synthetic microfibers are a major contributor to marine microplastic pollution, primarily originating from textiles. However, the mechanisms and rates of colored microfibers in marine environments remain unclear. This study systematically investigated the photoaging and release of microfibers from PET textiles in coastal seawater environments. Results demonstrated that 100 mg of PET textile released 1.44–4.74 × 10^4 microfibers after 12 d of UV exposure. This suggests that UV irradiation coupled with mechanical abrasion (induced by waves or tides) is an essential contributor to the formation of microfiber fragments in marine environments. In addition, dark-colored microfiber (e.g., purple and green) exhibited faster photoaging rates than light–colored ones (e.g., blue and yellow). This is due to the dark colored PET microfiber having a higher capacity to absorb UV light photons and producing more of the oxidative ROS (•OH) to accelerate the microfiber photoaging process. In further studies, contributions from the external factors (like biofouling, buoyancy changes, and marine transport behavior), rather than the sunlight-driven photoaging process, should also be investigated to fully understand the environmental behavior and ecological risks of microfibers in marine environments.

Overall, the findings presented in this study underscore the critical role of colored dye residues in PET textiles governing the microfiber formation in coastal seawater, which favors for unraveling the fate and ecological risks of surface-modified aged microfiber in marine ecosystems. Moreover, the color of dyes used in textiles is recommended to be considered when manufacturing PET commercial products (e.g., clothes, ropes, and filters). This will make great contributions in reducing and preventing the accumulation of microfibers in marine environments.

Supplementary information

It accompanies this paper at: https://doi.org/10.48130/newcontam-0025-0001.

Author contributions

The authors confirm their contributions to the paper as follows: conceptualization: Chen R, Zhao X; visualization, writing – draft manuscript preparation: Chen R; supervision: Zhao X; investigation: Wu X, Wang X, Wang J; funding acquisition: Wu X; writing – review & editing: Chen R, Zhao X, Wu X, Wang X, Wang J, Liang W. All authors reviewed the results and approved the final version of the manuscript.

Data availability

The datasets generated during and/or analyzed in the current study are available from the corresponding author on reasonable request.

Funding

This research was financially supported by the National Natural Science foundation of China (Grant No. 22406091, 41991315, and 41521003), Startup Foundation for Introducing Talent of Nanjing University of Information Science (2024r064), and Natural Science Foundation of Jiangsu Province (BK20240708).

Declarations

Competing interests

The authors declare that they have no conflict of interest.

Author details

[1]State Key Laboratory of Environmental Criteria and Risk Assessment, Chinese Research Academy of Environmental Sciences, Beijing 100012, China; [2]Jiangsu Key Laboratory of Atmospheric Environment Monitoring and Pollution Control, School of Environmental Science and Engineering, Nanjing University of Information Science and Technology, Nanjing 210044, China

References

[1] Thompson RC, Olsen Y, Mitchell RP, Davis A, Rowland SJ, et al. 2004. Lost at sea: where is all the plastic? *Science* 304:838

[2] Gong P, Xu H, Wang C, Chen Y, Guo L, et al. 2021. Persistent organic pollutant cycling in forests. *Nature Reviews Earth & Environment* 2:182–97

[3] Borrelle SB, Ringma J, Law KL, Monnahan CC, Lebreton L, et al. 2020. Predicted growth in plastic waste exceeds efforts to mitigate plastic pollution. *Science* 369:1515–18

[4] Wang C, O'Connor D, Wang L, Wu WM, Luo J, et al. 2022. Microplastics in urban runoff: global occurrence and fate. *Water Research* 225:119129

[5] Wang S, Gao L, Hou A, Xie K, Song X. 2021. Design, synthesis of novel bisazo disperse dyes: structure analysis and dyeing performance on PET. *Dyes and Pigments* 196:109761

[6] Barrows APW, Cathey SE, Petersen CW. 2018. Marine environment microfiber contamination: global patterns and the diversity of microparticle origins. *Environmental Pollution* 237:275–84

[7] Cheng H, Feng Y, Duan Z, Duan X, Zhao S, et al. 2021. Toxicities of microplastic fibers and granules on the development of zebrafish embryos and their combined effects with cadmium. *Chemosphere* 269:128677

[8] Qiao R, Deng Y, Zhang S, Wolosker MB, Zhu Q, et al. 2019. Accumulation of different shapes of microplastics initiates intestinal injury and gut microbiota dysbiosis in the gut of zebrafish. *Chemosphere* 236:124334

[9] Yang X, Man YB, Wong MH, Owen RB, Chow KL. 2022. Environmental health impacts of microplastics exposure on structural organization levels in the human body. *Science of the Total Environment* 825:154025

[10] Ergas M, Figueroa D, Paschke K, Urbina MA, Navarro JM, et al. 2023. Cellulosic and microplastic fibers in the Antarctic fish *Harpagifer antarcticus* and Sub-Antarctic *Harpagifer bispinis*. *Marine Pollution Bulletin* 194:115380

[11] Bai X, Li F, Ma L, Li C. 2022. Weathering of geotextiles under ultraviolet exposure: a neglected source of microfibers from coastal reclamation. *Science of the Total Environment* 804:150168

[12] Pinlova B, Nowack B. 2023. Characterization of fiber fragments released from polyester textiles during UV weathering. *Environmental Pollution* 322:121012

[13] Sun Y, Yuan J, Zhou T, Zhao Y, Yu F, et al. 2020. Laboratory simulation of microplastics weathering and its adsorption behaviors in an aqueous environment: a systematic review. *Environmental Pollution* 265:114864

[14] Qiu X, Ma S, Zhang J, Fang L, Guo X, et al. 2022. Dissolved organic matter promotes the aging process of polystyrene microplastics under dark and ultraviolet light conditions: the crucial role of reactive oxygen species. *Environmental Science & Technology* 56(14):10149–60

[15] Singh B, Sharma N. 2008. Mechanistic implications of plastic degradation. *Polymer Degradation and Stability* 93:561–84

[16] Liu S, Huang W, Yang J, Xiong Y, Huang Z, et al. 2023. Formation of environmentally persistent free radicals on microplastics under UV irradiations. *Journal of Hazardous Materials* 453:131277

[17] Zha F, Dai J, Han Y, Liu P, Wang M, et al. 2023. Release of millions of micro(nano)plastic fragments from photooxidation of disposable plastic boxes. *Science of the Total Environment* 858:160044

[18] Wang X, Zheng H, Zhao J, Luo X, Wang Z, et al. 2020. Photodegradation elevated the toxicity of polystyrene microplastics to grouper (*Epinephelus moara*) through disrupting hepatic lipid homeostasis. *Environmental Science & Technology* 54:6202–12

[19] Zou W, Xia M, Jiang K, Cao Z, Zhang X, et al. 2020. Photo-oxidative degradation mitigated the developmental toxicity of polyamide microplastics to zebrafish larvae by modulating macrophage-triggered proinflammatory responses and apoptosis. *Environmental Science & Technology* 54(21):13888–98

[20] Shi Y, Liu P, Wu X, Shi H, Huang H, et al. 2021. Insight into chain scission and release profiles from photodegradation of polycarbonate microplastics. *Water Research* 195:116980

[21] Zhao M, Huang L, Arulmani SRB, Yan J, Wu L, et al. 2022. Adsorption of different pollutants by using microplastic with different influencing factors and mechanisms in wastewater: a review. *Nanomaterials* 12:2256

[22] Pinlova B, Hufenus R, Nowack B. 2022. Systematic study of the presence of microplastic fibers during polyester yarn production. *Journal of Cleaner Production* 363:132247

[23] Du W, Zheng J, Li W, Liu Z, Wang H, et al. 2022. Efficient recognition and automatic sorting technology of waste textiles based on online near infrared spectroscopy and convolutional neural network. *Resources, Conservation and Recycling* 180:106157

[24] Ronda AC, Arias AH, Oliva AL, Marcovecchio JE. 2019. Synthetic microfibers in marine sediments and surface seawater from the Argentinean continental shelf and a Marine Protected Area. *Marine Pollution Bulletin* 149:110618

[25] Shi Y, Huang H, Zheng L, Tian Y, Gong Z, et al. 2023. Releases of microplastics and chemicals from nonwoven polyester fabric-based polyurethane synthetic leather by photoaging. *Science of the Total Environment* 902:166584

[26] Wu X, Zhao X, Chen R, Liu P, Liang W, et al. 2023. Size-dependent long-term weathering converting floating polypropylene macro- and microplastics into nanoplastics in coastal seawater environments. *Water Research* 242:120165

[27] Wu X, Liu P, Shi H, Wang H, Huang H, et al. 2021. Photo aging and fragmentation of polypropylene food packaging materials in artificial seawater. *Water Research* 188:116456

[28] Godlove IH. 1951. Improved color-difference formula, with applications to the perceptibility and acceptability of fadings. *Journal of the Optical Society of America* 41:760–72

[29] Moula ATMG, Hosen MD, Siddiquee MAB, Momin MA, Kaisar Z, et al. 2022. Effect of dye bath pH in dyeing of cotton knitted fabric with reactive dye (Remazol Yellow RR) in exhaust method: impact on color strength, chromatic values and fastness properties. *Heliyon* 8:e11246

[30] Du T, Shao S, Qian L, Meng R, Li T, et al. 2023. Effects of photochlorination on the physicochemical transformation of polystyrene nanoplastics: Mechanism and environmental fate. *Water Research* 243:120367

[31] Hua Z, Guo K, Kong X, Lin S, Wu Z, et al. 2019. PPCP degradation and DBP formation in the solar/free chlorine system: Effects of pH and dissolved oxygen. *Water Research* 150:77–85

[32] Enfrin M, Lee J, Gibert Y, Basheer F, Kong L, et al. 2020. Release of hazardous nanoplastic contaminants due to microplastics fragmentation under shear stress forces. *Journal of Hazardous Materials* 384:121393

[33] Zhang H, Huang Y, Zhou W. 2022. Prediction of the exposure endpoint of textile color fastness to light. *Journal of Physics: Conference Series* 2390:012047

[34] Sang T, Wallis CJ, Hill G, Britovsek GJP. 2020. Polyethylene terephthalate degradation under natural and accelerated weathering conditions. *European Polymer Journal* 136:109873

[35] Miranda MN, Sampaio MJ, Tavares PB, Silva AMT, Pereira MFR. 2021. Aging assessment of microplastics (LDPE, PET and uPVC) under urban environment stressors. *Science of the Total Environment* 796:148914

[36] Wang H, Liu P, Wang M, Wu X, Shi Y, et al. 2021. Enhanced phototransformation of atorvastatin by polystyrene microplastics: Critical role of aging. *Journal of Hazardous Materials* 408:124756

[37] Wu X, Zhao X, Chen R, Liu P, Liang W, et al. 2022. Wastewater treatment plants act as essential sources of microplastic formation in aquatic environments: a critical review. *Water Research* 221:118825

[38] Shi Y, Zheng L, Huang H, Tian YC, Gong Z, et al. 2023. Formation of nano- and microplastics and dissolved chemicals during photodegradation of polyester base fabrics with polyurethane coating. *Environmental Science & Technology* 57(5):1894–906

[39] Fontmorin JM, Burgos Castillo RC, Tang WZ, Sillanpää M. 2016. Stability of 5,5-dimethyl-1-pyrroline-*N*-oxide as a spin-trap for quantification of hydroxyl radicals in processes based on Fenton reaction. *Water Research* 99:24–32

[40] Garcia-Segura S, Brillas E. 2017. Applied photoelectrocatalysis on the degradation of organic pollutants in wastewaters. *Journal of Photochemistry and Photobiology C: Photochemistry Reviews* 31:1–35

[41] Ebrahimpour Z, Pliekhova O, Cabrera H, Abdelhamid M, Korte D, et al. 2021. Photodegradation mechanisms of reactive blue 19 dye under UV and simulated solar light irradiation. *Spectrochimica Acta Part A: Molecular and Biomolecular Spectroscopy* 252:119481

[42] Zhong J, Yang B, Feng Y, Chen Y, Wang LG, et al. 2021. Enhanced photo–Fenton removal efficiency with core-shell magnetic resin catalyst for textile dyeing wastewater treatment. *Water* 13:968

[43] Zhu K, Jia H, Zhao S, Xia T, Guo X, et al. 2019. Formation of environmentally persistent free radicals on microplastics under light irradiation. *Environmental Science & Technology* 53:8177–86